*International Journal of Computational and Experimental Science and ENgineering (IJCESEN)*

*Vol. 11-No.4 (2025) pp. 9864-9869*
*http://www.ijcesen.com*

***ISSN: 2149-9144***



**Research Article**

# FLUKA Monte Carlo Assessment of $Fe_2B$-Based Shielding Materials for Secondary Neutrons in a 1000 MeV Proton Accelerator

**Demet Sarıyer***

Manisa Celal Bayar University, Turgutlu Vocational High School, Turgutlu, Manisa, Turkey
**Corresponding Author Email:** demet.sariyer@cbu.edu.tr **ORCID:** 0000-0002-7803-111X

**Article Info:**

**DOI:** 10.22399/ijcesen.4544
**Received :** 05 October 2025
**Revised :** 29 November 2025
**Accepted :** 30 November 2025

**Keywords**

Neutron shielding,
Dose distribution,
FLUKA,
Ferroboron

**Abstract:**

High-energy proton accelerators generate high-energy neutrons through spallation processes, and these neutrons represent one of the most challenging particle types in terms of radiation shielding. In this study, secondary neutron dose distributions in the tunnel air environment at different distances and within the surrounding shielding structures were calculated for a 1000 MeV proton accelerator using FLUKA Monte Carlo simulations. Standard concrete, ferroboron ($Fe_2B$), and concrete doped with 20% $Fe_2B$ were considered as shielding materials, and their shielding performances at various thicknesses were comparatively evaluated. The simulation results demonstrate that $Fe_2B$ provides superior shielding performance compared to standard concrete and 20% $Fe_2B$-doped concrete, owing to its high effectiveness in moderating fast neutrons and absorbing thermal neutrons. In addition, an increase in shielding thickness was found to significantly reduce the measured dose levels. The findings indicate that $Fe_2B$-based materials constitute an effective and viable alternative for optimized shielding design in high-energy proton accelerator facilities.

## 1. Introduction

High-energy proton accelerators play a critical role in a wide range of advanced technological applications, including fundamental particle physics research, the development of intense neutron sources, medical isotope production, and radiation resistance testing [1-3]. In such systems, complex and multi-stage nuclear reactions occur as a result of interactions between protons with energies typically on the order of approximately 1 GeV and the target material. Among these reactions, the most prevalent is the spallation process, which consists of successive stages including the intranuclear cascade (INC), pre-equilibrium emission, and evaporation. During the early stages of spallation, high-energy protons penetrating the target nucleus undergo multiple collisions with nucleons, leading to the emission of secondary particles with a broad energy spectrum, particularly neutrons. These neutrons, especially those with high-energy components, pose significant radiological risks through both direct and indirect exposure pathways [4,5].

Because neutrons carry no electric charge, they do not interact via electromagnetic forces and can therefore travel considerable distances within materials compared to other types of ionizing radiation. This characteristic makes neutrons one of the most challenging radiation types to shield against. Effective control of neutron radiation originating from proton accelerators is essential to ensure personnel safety, protect accelerator components from radiation-induced damage, and maintain environmental radiation levels within permissible limits. In this context, the design of efficient neutron shielding systems represents a fundamental engineering requirement in high-energy accelerator facilities [4, 6, 7].

Conventional concrete, which is widely used in neutron shielding applications, contains medium-weight elements that are effective in moderating fast neutrons, as well as light elements that contribute to the attenuation of low-energy neutrons [8]. However, due to their relatively low density, standard concrete requires large structural thicknesses to achieve sufficient shielding performance, thereby limiting both structural efficiency and economic feasibility. The fundamental approach to neutron shielding involves the moderation of fast neutrons using hydrogen-rich materials and the absorption of

thermal neutrons by elements with high neutron capture cross sections [5,9]. Accordingly, specialized concrete mixtures with enhanced shielding performance have been developed by incorporating high-density iron and boron-containing ferroboron (FeB, $Fe_2B$), which is highly effective in neutron absorption, into standard concrete compositions [1,5, 10, 11]. These modified concretes not only provide more effective shielding across a broad neutron energy spectrum but also enhance radiological safety in accelerator-based nuclear facilities and contribute to the long-term mechanical durability of structural components [12, 13].

Monte Carlo-based particle transport codes, such as FLUKA, GEANT4, MCNPX, and PHITS, are widely employed in the design and optimization of radiation shielding systems. These computational tools offer high accuracy and reliability in determining dose distributions, modeling secondary radiation production, and calculating optimal shielding thicknesses [5, 14, 15].

In this study, current approaches to the shielding of secondary neutrons generated by spallation processes in 1000 MeV proton accelerators are investigated. The neutron shielding performances of standard concrete, $Fe_2B$, and concrete doped with 20% $Fe_2B$ are comparatively analyzed using FLUKA Monte Carlo simulations. Dose distributions within the tunnel air environment and inside the surrounding shielding structures are evaluated to identify the most effective shielding material.

## 2. Material and Methods

Within the scope of this study, a tunnel-type shielding geometry was modeled to estimate the dose distributions of secondary neutrons generated under abnormal operating conditions in accelerator facilities employing 1000 MeV proton beams. Standard concrete, $Fe_2B$, and concrete doped with 20% $Fe_2B$ were considered as shielding materials. The shielding design and dose calculations were carried out using the FLUKA Monte Carlo simulation code, versions 2011.2b and 2011.2c.

### 2.1 Simulation Design and Data Generation Using the FLUKA Monte Carlo Code

The tunnel design was developed to account for neutrons generated by proton interactions with a copper target under abnormal operating conditions of the accelerator. The proton beam was modeled as a point source. In order to ensure that the dose rate outside the tunnel shielding surrounding the copper target remained below the maximum permissible limits, a sufficiently large shielding thickness was selected in the simulation geometry. In the geometric definition of the model, a spherical geometry with a radius of 25 m was defined to allow particle interactions within the specified environment. A 1 m thick black-body boundary was applied to the outer layer of this sphere to terminate particle tracking. Standard concrete, $Fe_2B$, and concrete doped with 20% $Fe_2B$ were employed as shielding materials, and the total shielding thickness was set to 24 m. Within this spherical geometry, a tunnel filled with air and having dimensions of 5 m × 5 m × 10 m was modeled.

During proton transport inside the tunnel, copper - commonly used for the inner surfaces of accelerator components in regions where beam losses occur - was selected as the target material. The target was modeled as a rectangular copper block with dimensions of 5 cm × 5 cm ×5 cm. To determine the maximum dose levels, a point source was positioned at the geometric center of the copper target. Furthermore, to prevent direct interaction and activation of the shielding material by the proton beam, the beam axis was positioned at distances of 2.5 m from the side walls and 4 m from the upper wall.

Due to the statistical nature of the Monte Carlo method, a large number of particle histories are required to achieve high accuracy. Accordingly, to reduce statistical uncertainties in the calculations, the simulations were performed in five independent cycles using different random number seeds, each consisting of $6\times10^8$ primary particles. Owing to the high particle energy and large number of histories, the simulations required substantial computational resources and were carried out on the TR-GRID national high-performance computing cluster.

The simulation outputs were analyzed in detail using FLUKA output files. To determine dose values at different distances within the tunnel air environment and across varying thicknesses of standard concrete, $Fe_2B$ and 20% $Fe_2B$-doped concrete shielding, the USRBIN detector card was employed. The detector dimensions were defined as 3400 cm, 3000 cm, and 1900 cm along the x, y and z - axes, with corresponding bin numbers of 340, 300, and 190. This configuration resulted in detector voxel dimensions of $10\times10\times10$ $cm^3$.

In the FLUKA simulations, dose equivalents were calculated using the USRBIN scoring card by convoluting particle fluence with the fluence-to-dose-equivalent conversion coefficients implemented in FLUKA. The proton energy was set to 1000 MeV, and the resulting dose distributions were visualized and analyzed using FLUKA' s graphical user interface, FLAIR. The

dose distribution curves of secondary neutrons on the xy-plane, generated by proton-target interactions at a proton energy of 1000 MeV in the tunnel air environment and within different surrounding shielding materials, are presented in Fig.1(a-c) for the following shielding configurations: (a) standard concrete, (b) $Fe_2B$, and (c) concrete doped with 20% $Fe_2B$.

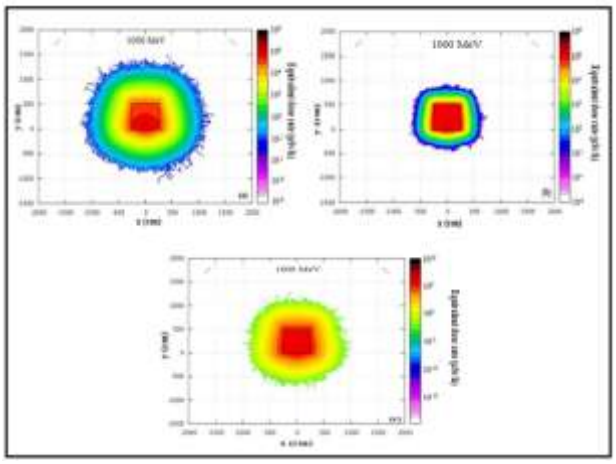

***Figure 1.*** *xy-plane dose distribution of secondary neutrons in the tunnel air and surrounding shielding environment - (a) standard concrete, (b) $Fe_2B$, and (c) concrete doped with 20% $Fe_2B$ - for a 1000 MeV proton accelerator.*

For the shielding configurations consisting of standard concrete, $Fe_2B$, and concrete doped with 20% $Fe_2B$, the radial dose values obtained at different distances within the tunnel air environment and inside the surrounding shielding materials are comparatively presented and analyzed in Fig.2 and 3.

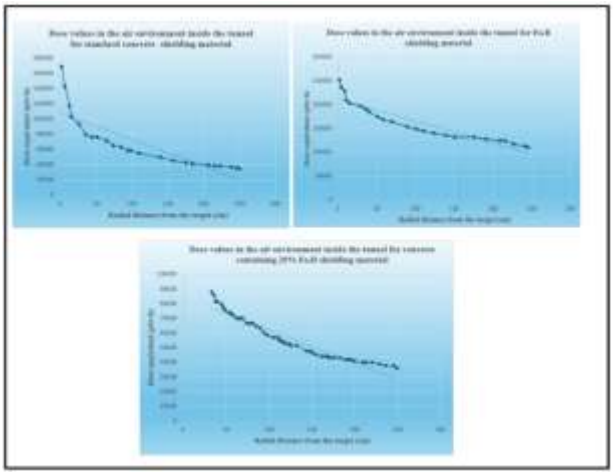

***Figure 2.*** *Radial dose distributions obtained at different distances in the tunnel air environment for shielding configurations consisting of standard concrete, $Fe_2B$, and concrete doped with 20% $Fe_2B$.*

Fig. 2 presents the secondary neutron radial dose distributions obtained at different distances from the target center in the tunnel air environment for shielding configurations composed of standard concrete, $Fe_2B$, and concrete doped with 20% $Fe_2B$. For all shielding types, the dose values reach their maximum levels in regions close to the target and exhibit a pronounced decrease with increasing radial distance. This behavior is consistent with the attenuation of neutrons due to scattering, energy loss, and interactions within the air environment and the surrounding shielding materials.

In the case of standard concrete shielding, although the dose levels decrease with distance, relatively higher dose values are maintained near the target compared to the other shielding materials. This observation can be attributed to the limited effectiveness of standard concrete in moderating high-energy neutrons and absorbing thermal neutrons.

When $Fe_2B$ is employed as the shielding material, significantly lower dose values are observed over the entire radial distance range compared to standard concrete. This result highlights the enhanced neutron attenuation capability of $Fe_2B$, which arises from the high thermal neutron capture cross section of boron combined with the contribution of iron to the energy degradation of fast neutrons.

The concrete doped with 20% $Fe_2B$ exhibits an intermediate shielding performance between standard concrete and pure $Fe_2B$. The corresponding dose distributions indicate a substantial improvement relative to standard concrete; however, the attenuation levels do not fully reach those achieved with $Fe_2B$ shielding. Nevertheless, considering the structural and economic advantages of doped concrete, this configuration can be regarded as a balanced and practical alternative for shielding applications.

Overall, the results shown in Fig. 2 clearly demonstrate that $Fe_2B$-based shielding materials provide more effective radiation protection against secondary neutrons generated in high-energy proton accelerator facilities. Furthermore, the findings emphasize that the composition of the shielding material plays a critical role in determining dose levels within the tunnel environment, supporting the use of $Fe_2B$ and $Fe_2B$-doped concrete as strong candidates for optimized shielding design. The $Fe_2B$ shielding configuration demonstrates the most significant dose reduction across all radial distances. The steep decline in dose within the initial shielding layers highlights the superior neutron attenuation performance of $Fe_2B$, which can be attributed to the combined effects of iron in degrading the energy of fast neutrons and boron in efficiently capturing thermalized neutrons.

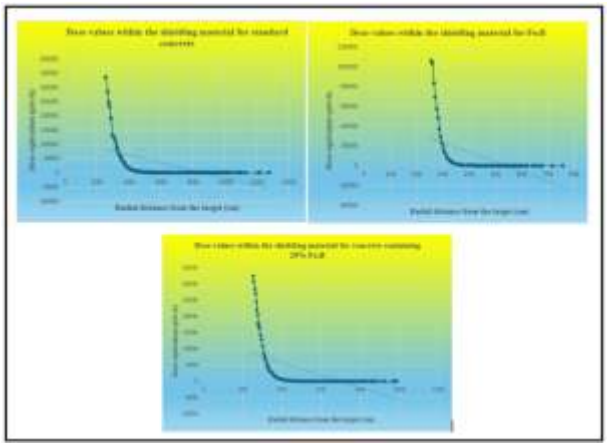

***Figure 3.*** *Radial dose distributions obtained for different shielding thicknesses in tunnel-surrounding environments composed of standard concrete, $Fe_2B$, and concrete doped with 20% $Fe_2B$.*

Consequently, $Fe_2B$ provides a more compact and efficient shielding solution compared to standard concrete.

For concrete containing 20% $Fe_2B$, the dose distributions lie between those of standard concrete and pure $Fe_2B$ shielding. A substantial improvement over standard concrete is evident, particularly in the near-shielding region, indicating that the incorporation of $Fe_2B$ significantly enhances neutron attenuation. Although its performance does not fully match that of pure $Fe_2B$, the doped concrete offers a favorable compromise between shielding efficiency, structural applicability, and material feasibility.

Overall, the results presented in Fig. 3 clearly demonstrate that both the shielding thickness and material composition play a decisive role in controlling neutron dose levels in tunnel-surrounding environments. $Fe_2B$-based materials, either as pure shielding or as concrete additives, markedly improve shielding effectiveness and represent promising candidates for optimized radiation protection in high-energy proton accelerator facilities.

## 3. Results and Discussions

In this study, dose distributions of secondary neutrons generated by proton–target interactions at a proton energy of 1000 MeV were investigated in detail using FLUKA Monte Carlo simulations for different shielding materials and shielding thicknesses. Radial dose values obtained for shielding configurations consisting of standard concrete, $Fe_2B$, and concrete doped with 20% $Fe_2B$ were comparatively evaluated both in the tunnel air environment and within the surrounding shielding materials.

### 3.1. Radial Dose Distributions in the Tunnel Air Environment

Fig. 2 presents the radial dose distributions of secondary neutrons obtained at different distances from the target center in the tunnel air environment for shielding configurations composed of standard concrete, $Fe_2B$, and concrete doped with 20% $Fe_2B$. For all shielding types, the dose values reach their maximum levels in regions close to the target and decrease significantly with increasing radial distance. This trend can be attributed to neutron attenuation resulting from scattering, energy loss, and interactions within the air environment and the surrounding shielding materials.

For the standard concrete shielding configuration, although the dose levels decrease with distance, relatively higher dose values are observed near the target compared to the other shielding materials. This behavior indicates the limited effectiveness of standard concrete in moderating high-energy neutrons and absorbing thermal neutrons.

In contrast, the $Fe_2B$ shielding configuration exhibits substantially lower dose levels over the entire radial distance range. This pronounced reduction highlights the superior neutron attenuation capability of $Fe_2B$, which arises from the combined effects of iron in degrading the energy of fast neutrons and boron in efficiently capturing thermalized neutrons. Consequently, $Fe_2B$ emerges as the most effective shielding material in reducing secondary neutron doses within the tunnel air environment.

The concrete doped with 20% $Fe_2B$ demonstrates an intermediate performance between standard concrete and pure $Fe_2B$. While a significant improvement in dose reduction relative to standard concrete is achieved, the attenuation levels remain lower than those obtained with pure $Fe_2B$ shielding. Nevertheless, considering its structural integrity and economic feasibility, $Fe_2B$-doped concrete represents a practical and balanced alternative for shielding applications.

### 3.2. Radial Dose Distributions within the Shielding Materials

Fig. 3 shows the radial dose distributions obtained within the tunnel-surrounding shielding materials for different shielding thicknesses. For all shielding configurations, the dose values decrease rapidly within the initial layers of the shielding and gradually reach lower and more stable levels at larger radial distances. This behavior reflects the successive scattering, moderation, and absorption processes experienced by secondary neutrons as they propagate through the shielding materials.

Among the investigated materials, the $Fe_2B$ shielding configuration provides the highest dose attenuation across all shielding thicknesses. The steep dose reduction observed near the target region demonstrates the superior shielding efficiency of $Fe_2B$ against high-energy neutrons, enabling more compact shielding designs.
For concrete containing 20% $Fe_2B$, the dose distributions indicate a clear improvement over standard concrete, particularly in the near-shielding regions. However, its performance does not fully match that of pure $Fe_2B$ shielding. Despite this limitation, $Fe_2B$-doped concrete effectively reduces neutron doses with increasing thickness and offers a viable compromise between shielding efficiency and practical applicability in engineering designs.

### 3.3. General Assessment

Overall, the results clearly demonstrate that both shielding thickness and material composition play a decisive role in controlling neutron dose levels in the tunnel air environment and within the surrounding shielding structures. While pure $Fe_2B$ provides the highest attenuation performance, concrete doped with 20% $Fe_2B$ offers a balanced solution by combining enhanced shielding capability with structural and economic advantages. These findings indicate that $Fe_2B$-based materials are strong candidates for optimized radiation shielding in high-energy proton accelerator facilities

## 4. Conclusions

In this study, the shielding performance of standard concrete, $Fe_2B$, and concrete doped with 20% $Fe_2B$ against secondary neutrons generated by 1000 MeV proton–target interactions was investigated using FLUKA Monte Carlo simulations. The results indicate that $Fe_2B$ exhibits superior shielding performance compared to standard concrete across all investigated regions, primarily due to the effective moderation of fast neutrons and the high thermal neutron capture capability of boron. Concrete containing 20% $Fe_2B$ provides a significant dose reduction relative to standard concrete while offering a balanced solution in terms of structural applicability and cost. Accordingly, the findings demonstrate that material composition and shielding thickness play a decisive role in neutron shielding design, and that $Fe_2B$-based materials represent promising alternatives for effective radiation protection in high-energy proton accelerator facilities. More works done on similar topics[16-19].

## Author Statements:

- **Ethical approval:** The conducted research is not related to either human or animal use.
- **Conflict of interest:** The authors declare that they have no known competing financial interests or personal relationships that could have appeared to influence the work reported in this paper
- **Acknowledgement:** The numerical calculations reported in this paper were performed at TUBITAK ULAKBIM, High Performance and Grid Computing Center (TRUBA Resources).
- **Author contributions:** The authors declare that they have equal right on this paper.
- **Funding information:** The authors declare that there is no funding to be acknowledged.
- **Data availability statement:** The data that support the findings of this study are available on request from the corresponding author. The data are not publicly available due to privacy or ethical restrictions.

## References

[1] Sariyer, D., & Küçer, R. (2020). Effect of different materials to concrete as neutron shielding application. *Acta Physica Polonica A, 137*(4, Special Issue: ICCESEN-2019), 477–480. https://doi.org/10.12693/APhysPolA.137.477

[2] Emikönel, S., & Akkurt, İ. (2025). Radiation shielding properties of $B_2O_3$–$Bi_2O_3$ glass. *International Journal of Computational and Experimental Science and Engineering (IJCESEN), 11*(2). https://doi.org/10.22399/ijcesen.2157

[3] Soyal, H., & Sarıhan, M. (2025). Evaluation of radiation protection knowledge and attitudes of health services vocational school students participating in practice in radiated environments. *International Journal of Computational and Experimental Science and Engineering (IJCESEN), 11*(2). https://doi.org/10.22399/ijcesen.508

[4] Liu, J. (2005). Nuclear reactions: Spallation physics and ADS target design. *Brazilian Journal of Physics, 35*(3B), 894–902. https://doi.org/10.1590/S0103-97332005000500048

[5] Sarıyer, D. (2017). *Proton hızlandırıcılarında tünel tasarımı için kullanılan farklı zırh maddelerinin doz dağılımlarına etkileri* (Doktora tezi). Manisa Celal Bayar Üniversitesi, Fen Bilimleri Enstitüsü, Manisa, Türkiye.

[6] Sarkar, P. K. (2010). Neutron dosimetry in the particle accelerator environment. *Radiation Measurements, 45*(10), 1476–1483. https://doi.org/10.1016/j.radmeas.2010.07.001

[7] Paul, M. B., Dutta Ankan, A., Deb, H., & Ahasan, M. M. (2023). A Monte Carlo simulation model to determine the effective concrete materials for fast neutron shielding. *Radiation Physics and Chemistry, 202*, 110476. https://doi.org/10.1016/j.radphyschem.2022.110476

[8] Waheed, F., Al-Sudani, M. A. M., & Akkurt, I. (2025). The experimental enhancing of the radiation shield properties of some produced compounds. *International Journal of Applied Sciences and Radiation Research (IJASRaR), 2*(1). https://doi.org/10.22399/ijasrar.1

[9] Sarıyer, D., Küçer, R., & Küçer, N. (2015). Neutron shielding properties of concrete and ferro-boron. *Acta Physica Polonica A, 128*(2-B), B-201. https://doi.org/10.12693/APhysPolA.128.B-201

[10] Sarıyer, D., Küçer, R., & Küçer, N. (2015). Neutron shielding properties of concretes containing boron carbide and ferro-boron. *Procedia – Social and Behavioral Sciences, 195*, 1752–1756. https://doi.org/10.1016/j.sbspro.2015.06.320

[11] Sariyer, D., & Küçer, R. (2018). Development of neutron shielding concrete containing iron content materials. *AIP Conference Proceedings, 1935*(1), 100003. https://doi.org/10.1063/1.5025991

[12] Barbhuiya, S., Das, B. B., Norman, P., & Qureshi, T. (2024). A comprehensive review of radiation shielding concrete: Properties, design, evaluation, and applications. *Structural Concrete*. https://doi.org/10.1002/suco.202400519

[13] Gharieb, M., Mosleh, Y. A., Alwetaishi, M., Hussein, E. E., & Sultan, M. E. (2021). Effect of using heavy aggregates on the high performance concrete used in nuclear facilities. *Construction and Building Materials, 310*, 125111. https://doi.org/10.1016/j.conbuildmat.2021.125111

[14] Rokni, S. H., Cossairt, J. D., & Liu, J. C. (2007). *Radiation shielding at high-energy electron and proton accelerators* (SLAC Report). Stanford Linear Accelerator Center.

[15]Hançerlioğulları, A. (2006). Monte Carlo simulation method and the MCNP code system. *Kastamonu Education Journal, 14*(2), 545–556.

[16]Günoğlu, K., & Akkurt, İskender. (2023). Gamma-ray attenuation properties carbide compounds (WC, Mo2C, TiC, SiC, B4C) using Phy-X/PSD software. *International Journal of Applied Sciences and Radiation Research , 1*(1), 1–8. https://doi.org/10.22399/ijasrar.6

[17]Waheed, F., Mohamed Abdulhusein Mohsin Al-Sudani, & Iskender Akkurt. (2025). The Experimental Enhancing of the Radiation Shield Properties of Some Produced Compounds. *International Journal of Applied Sciences and Radiation Research , 2*(1). https://doi.org/10.22399/ijasrar.1

[18]Vural, M., Kabaca, A., Aksoy, S. H., Demir, M., Karaçam, S. Çavdar, Ulusoy, İdil, … Günay, O. (2025). Determination Of Radiation Dose Levels to Which Partois And Spinal Cord (C1-C2) Regions Are Exposed In Computed Tomography Brain Imaging. *International Journal of Applied Sciences and Radiation Research , 2*(1). https://doi.org/10.22399/ijasrar.17

[19]Morad Kh. Hamad. (2025). Synergistic Evaluation of Ionizing Radiation Shielding in Novel Lead-Free Alloys Using Geant4 MC toolkit. *International Journal of Applied Sciences and Radiation Research , 2*(1). https://doi.org/10.22399/ijasrar.47